What can be learned from binding energy differences about nuclear structure: The example of δV_{pn}

M. Bender[1,2] and P.-H. Heenen[3]

[1]*Centre d'Etudes Nucléaires de Bordeaux Gradignan, UMR5797, Université Bordeaux, F-33175 Gradignan, France*

[2]*CNRS/IN2P3, Centre d'Etudes Nucléaires de Bordeaux Gradignan, UMR5797, F-33175 Gradignan, France*

[3]*Physique Nucléaire Théorique, CP229, Université Libre de Bruxelles, B-1050 Bruxelles, Belgium*

(Received 8 February 2011; published 17 June 2011)

We perform an analysis of a binding energy difference called $\delta V_{pn}(N, Z) \equiv -\frac{1}{4}[E(Z, N) - E(Z, N-2) - E(Z-2, N) + E(Z-2, N-2)]$ in the framework of a realistic nuclear model. It has been suggested that δV_{pn} values provide a sensitive probe of nuclear structure, and it has been put forward as a primary motivation for the measurement of specific nuclear masses. Using the angular momentum and particle-number projected generator coordinate method and the Skyrme interaction SLy4, we analyze the contribution brought to δV_{pn} by static deformation and dynamic fluctuations around the mean-field ground state. Our method gives a good overall description of δV_{pn} throughout the chart of nuclei with the exception of the anomaly related to the Wigner energy along the $N = Z$ line. The main conclusions of our analysis of δV_{pn}, which are at variance with its standard interpretation, are that (i) the structures seen in the systematics of δV_{pn} throughout the chart of nuclei can be easily explained combining a smooth background related to the symmetry energy and correlation energies due to deformation and collective fluctuations, (ii) the characteristic pattern of δV_{pn} having a much larger size for nuclei that add only particles or only holes to a doubly magic nucleus than for nuclei that add particles for one nucleon species and holes for the other is a trivial consequence of the asymmetric definition of δV_{pn} and not due to a the different structure of these nuclei, (iii) δV_{pn} does not provide a very reliable indicator for structural changes, (iv)δV_{pn} does not provide a reliable measure of the proton-neutron interaction in the nuclear energy density functional (EDF) or of that between the last filled orbits or of the one summed over all orbits, and (v) δV_{pn} does not provide a conclusive benchmark for nuclear EDF methods that is superior or complementary to other mass filters such as two-nucleon separation energies or Q values.

DOI: 10.1103/PhysRevC.83.064319 PACS number(s): 21.10.Dr, 21.60.Jz

I. INTRODUCTION

Nuclear masses are currently measured with an unprecedented accuracy [1–4], in many cases better than a few keV. Such an accuracy is obtained not only for nuclei close to the stability line but also for exotic ones with very short lifetimes. A recurrent question is how to take advantage of this major advance and how to use it to improve the theoretical description of nuclear ground states.

The first possibility is to compare masses, or even better binding energies, directly to theoretical predictions. Unfortunately, *ab initio* methods based on a realistic nucleon-nucleon interaction are not available for systematic studies of heavy nuclei. If they were, any disagreement with the experimental data would point to a deficiency of the interaction. When the many-body problem is not solved exactly (or, to be more precise, with a controlled numerical accuracy) but with an effective model using effective degrees of freedom and an effective interaction, the link between data and nucleon-nucleon interaction is broken, and a discrepancy between calculation and experiment can have its source in any ingredient of the model.

The best available theoretical descriptions of masses [1,5–8] are not based on *ab initio* methods. The three main models rely on very different ingredients. The mass formula of Duflo and Zuker [5] does not make an explicit reference to a nucleon-nucleon interaction. Nevertheless, it assumes that there exist effective interactions smooth enough for Hartree-Fock calculations to be possible. The corresponding Hamiltonian is separated into monopole and multipole terms that are parameterized through scaling and symmetry arguments [1]. The macroscopic-microscopic approaches of Möller *et al.* [6] combine a finite-range liquid-drop or droplet model and shell effects introduced through the Strutinsky shell correction method and a parameterized one-body potential. The main ingredient of the Hartree-Fock-Bogoliubov (HFB) mass formulas of Goriely *et al.* is an energy density functional (EDF), which is widely used in self-consistent mean-field calculations. In a first variant, a Skyrme EDF is supplemented by empirical corrections for correlations that cannot be included in a mean field [7]. In a second variant, the same Gogny interaction is used to determine the mean field and quadrupole correlation effects beyond the mean field through a microscopic Bohr Hamiltonian [8]. The comparison of any of these models with data can hardly allow us to extract general information about the nucleon-nucleon interaction. Comparison with results obtained using *ab initio* methods and realistic interactions can be made through the idealized model of infinite nuclear matter. From such calculations, one can extract specific parameters, such as volume and symmetry energy coefficients, corresponding to a liquid-drop formula (LDM) fitted to masses. Here also, the connection between theory and experiment is ambiguous. The liquid-drop model is justified by a leptodermous expansion of the energy that cannot be expected to converge quickly even for the heaviest nuclei [9,10].

An apparently more appealing way to proceed is to relate differences between binding energies of neighboring nuclei to

specific features of nuclear models, in particular to effective single-particle energies or effective two-body matrix elements [11]. Models that fail to reproduce masses with a good accuracy are often more reliable for mass differences. The reason for this success is that mass residuals $M_{\rm th} - M_{\rm expt}$ for adjacent nuclei are not independent in a given mass model [12,13].

This property has been used for a long time to associate one-nucleon separation energies with single-particle energies or higher-order differences with pairing gaps. In particular, two-particle separation energies are important indicators of shell closures. One has to distinguish, however, between the use of mass filters as *measures* of specific model ingredients and their use as *signatures* of structural changes. In particular, a mass filter cannot be expected to provide both simultaneously. One can test a model ingredient only when all nuclei entering a mass filter have the same structure, which becomes increasingly improbable with the number of nuclei involved. In contrast, the indication of a structural change (such as onset of deformation) by a mass filter often means that the fundamental assumptions made for its direct association with a feature of a model are violated.

In a previous paper [14], we discussed the difficulties encountered when trying to relate structures seen in the systematics of energy differences to features of the single-particle levels. The changes in the large gaps observed in data for two-neutron or two-proton separation energies are often interpreted as being due to the evolution of shell structure with N and Z and associated with the presence of strong residual tensor interactions [15] or a weakening of the spin-orbit interaction in neutron-rich nuclei [16,17]. We showed that experimental data can be explained in a coherent way within mean-field-based models as being due to a combination of the slow modification of spherical single-particle spectra and the often rapid variation of collective correlation effects.

In this paper, we perform a similar analysis for a mass filter that has become fashionable and has been identified with the proton-neutron interaction in nuclei. Many recent experimental data have been used to interpret a difference between the (negative) binding energies of four even-even nuclei defined as

$$\delta V_{pn}(N,Z) = -\tfrac{1}{4}[E(Z,N) - E(Z,N-2) - E(Z-2,N) + E(Z-2,N-2)] \quad (1)$$

in terms of the effective interaction between the last occupied neutron and proton orbits [18–25]. A similar quantity has been analyzed in great detail by Jänecke *et al.* [26], but for nuclei differing by one neutron and/or one proton only, which makes its interpretation more difficult. Indeed, the breaking of a pair in a nucleus with an odd number of particles modifies pairing correlations deeply and makes the structure of its wave function significantly different from that of its even neighbors. By comparing only nuclei with an even number of neutrons and protons, one can hope that the assumption of a common mean field is better justified. Differences between two consecutive δV_{pn} values have also been proposed as a measure for the Wigner energy that leads to an anomaly of binding energies around the $N = Z$ line [27,28].

In Sec. II, we show how, in the framework of the Hartree-Fock (HF) method, δV_{pn} can be related to the interaction between the last filled neutron and proton orbits when making the same assumptions as those used to derive Koopman's theorem [29]. We show that the introduction of pairing correlations and density dependencies complicates the relation even when making oversimplifying assumptions about the evolution of wave functions with N and Z. We discuss the main effects that make any direct identification of δV_{pn} with a proton-neutron interaction doubtful. In Sec. IV, we present results obtained from calculations using a realistic microscopic model using the Skyrme energy density functional SLy4. We demonstrate how the successive inclusion of correlations from spherical to deformed mean-field calculations and further to symmetry restoration and configuration mixing permits us to improve at each step the agreement with the experimental data while, at the same time, losing in an ever-increasing manner the simple interpretation of δV_{pn}. Section V summarizes our findings.

II. ANALYSIS OF δV_{pn}

Surprisingly, the abundant literature discussing the relevance of δV_{pn} contains only a very few analyses of its relation with the proton-neutron interaction in nonschematic models. Exceptions are the shell-model study of Heyde *et al.* [30], who underline that a simple interpretation of δV_{pn} can only be given when there is just one dominant orbital for protons and neutrons each, and the nuclear Density Functional Theory study by Stoitsov *et al.* [24], who, however, focus their analysis on the overall excellent reproduction of data for δV_{pn} with their model, rather than on the ingredients of the model that contribute to it. Below, we review the assumptions to be made to relate δV_{pn} to the effective proton-neutron interaction in finite nuclei and discuss their validity in the context of realistic nuclear models based on the self-consistent mean field and taking the entire space of occupied single-particle orbits into account. We start with a simple two-body Hamiltonian and discuss the corresponding energy in the context of HF (without pairing) and HFB (with pairing). Then, we generalize the discussion to a more realistic effective interaction that includes three-body forces or density dependencies.

A. Frozen HF with two-body interaction

Let us start from a Hamiltonian consisting of a kinetic energy term and an antisymmetrized two-body interaction:

$$\hat{H} = \sum_{i,j} t_{ij} a_i^\dagger a_j + \frac{1}{4} \sum_{i,j,m,n} \bar{v}_{ijmn}\, a_i^\dagger a_j^\dagger a_n a_m \,. \quad (2)$$

When limiting the N-body wave function to a single Slater determinant, the minimum value of the energy is obtained by solving HF equations [29]. In this case the energy for a nucleus

consisting of N neutrons and Z protons is given by

$$E^{\rm HF}(N,Z) = \sum_{n=1}^{N} t_{nn}^{N,Z} + \sum_{p=1}^{Z} t_{pp}^{N,Z} + \frac{1}{2}\sum_{n,n'=1}^{N} \bar{v}_{nn'nn'}^{N,Z} + \frac{1}{2}\sum_{p,p'=1}^{Z} \bar{v}_{pp'pp'}^{N,Z} + \sum_{n=1}^{N}\sum_{p=1}^{Z} \bar{v}_{npnp}^{N,Z}, \quad (3)$$

where $t_{nn}^{N,Z}$ are the matrix elements of the kinetic energy operator and $\bar{v}_{nn'nn'}^{N,Z}$ are the matrix elements of the two-body interaction calculated in the single-particle basis that solves the HF equations. We have added superscripts N, Z to these matrix elements to recall that the HF equations are solved self-consistently and that, in general, the wave functions differ for each combination of N and Z values.

Let us assume for the moment that the HF single-particle basis is identical for the four nuclei with (N, Z), $(N-2, Z)$, $(N, Z-2)$, and $(N-2, Z-2)$. This "frozen HF" approximation leads to

$$\delta V_{pn}^{\rm HF_{frozen}}(N,Z) = -\tfrac{1}{4}\,(\bar{v}_{N-1,Z-1,N-1,Z-1} + \bar{v}_{N-1,Z,N-1,Z} + \bar{v}_{N,Z-1,N,Z-1} + \bar{v}_{N,Z,N,Z}). \quad (4)$$

The superscripts have been dropped, as the mean field is supposed to be the same for the four nuclei.[1]

A further simplification can be obtained by noting that, for even N and Z, the two valence neutrons (indices $N-1$ and N) and protons (indices $Z-1$ and Z) occupy time-reversed orbits in the HF solution and that the matrix elements are equal two by two:

$$\delta V_{pn}^{\rm HF_{frozen}}(N,Z) = -\tfrac{1}{2}(\bar{v}_{N,Z-1,N,Z-1} + \bar{v}_{N,Z,N,Z}). \quad (5)$$

Even in this simple case, the final result is not a single matrix element but a combination of matrix elements between the valence particles.

This derivation requires the same assumptions as those made to derive Koopman's theorem [29], which relates single-particle energies and one-nucleon separation energies. Koopman's theorem, however, is known to have a very limited validity in nuclear physics (see the discussion in Ref. [14] and references therein).

B. Frozen HF + BCS and HFB with two-body interaction

It is obvious that the assumptions made in the previous section will rarely be justified, even approximately. Let us first examine the consequence of the partial occupation of single-particle levels due to pairing correlations. We consider only pure proton-proton and neutron-neutron pairing, which can be justified for nuclei with N sufficiently different from Z. In the presence of proton-neutron pairing, the many-body state could not be written as the direct product of a proton and a neutron BCS state, and the energy would not be separable into proton and neutron components any longer.

The HF + BCS or HFB expectation value of a two-body Hamiltonian (2) for a nucleus with N neutrons and Z protons evaluated in the canonical basis is given by

$$\begin{aligned} E^{\rm HFB}(N,Z) &= \sum_{n} t_{nn}^{N,Z}\, v_{n,N}^2 + \sum_{p} t_{pp}^{N,Z}\, v_{p,Z}^2 + \frac{1}{2}\sum_{n,n'} \bar{v}_{nn'nn'}^{N,Z}\, v_{n,N}^2\, v_{n',N}^2 \\ &+ \sum_{n}\sum_{p} \bar{v}_{npnp}^{N,Z}\, v_{n,N}^2\, v_{p,Z}^2 + \frac{1}{2}\sum_{p,p'} \bar{v}_{pp'pp'}^{N,Z}\, v_{p,Z}^2\, v_{p',Z}^2 \\ &+ \sum_{n,n'>0} \bar{v}_{n\bar{n}n'\bar{n}'}^{N,Z}\, u_{n,N}\, v_{n,N}\, v_{n',N}\, v_{n',N} \\ &+ \sum_{p,p'>0} \bar{v}_{p\bar{p}p'\bar{p}'}^{N,Z}\, u_{p,Z}\, v_{p,Z}\, v_{p',Z}\, v_{p',Z}\,. \end{aligned} \quad (6)$$

The u_k and v_k are real occupation amplitudes with $u_k = u_{\bar{k}} > 0$, $v_k = -v_{\bar{k}}$, and $u_k^2 + v_k^2 = 1$. Indices k and $\bar{k}$ refer to conjugate states, which for the ground states of even-even nuclei are connected by the time-reversal operator. We use the usual convention where summation over all indices indicates summation over all k and $\bar{k}$, whereas summation over "positive" indices means that the sums are over all k but not their conjugate levels $\bar{k}$. The second index of the occupation amplitudes recalls that these are occupation numbers for a nucleus with $\sum_n v_{n,N}^2 = N$ neutrons and $\sum_p v_{p,Z}^2 = Z$ protons. Except for the last two terms, the summation runs over positive and negative values of n and p.

To derive a simple expression for δV_{pn}, a similar assumption as in the frozen HF case has to be made, namely, that the canonical single-particle basis is the same for all four nuclei entering a given $\delta V_{pn}(N,Z)$. In this case, the matrix elements t_{kk} and $\bar{v}_{kk'kk'}$ do not depend on N and Z. In addition, one has to assume that the solution of the HFB equations for neutron states does not depend on the number of protons and vice versa. This leads to

$$\delta V_{pn}^{\rm HFB_{frozen}}(N,Z) = -\frac{1}{4}\sum_{n}\sum_{p} \bar{v}_{npnp}\, \Delta v_{n,N}^2\, \Delta v_{p,Z}^2\,, \quad (7)$$

where we introduced the shorthand $\Delta v_{n,N}^2 \equiv v_{n,N}^2 - v_{n,N-2}^2$ for the change of neutron occupation numbers when removing two neutrons, $\sum_n \Delta v_{n,N}^2 = 2$, and its homologue $\Delta v_{p,Z}^2 \equiv v_{p,Z}^2 - v_{p,Z-2}^2$ for protons.

C. Frozen HF with three-body or density-dependent interactions

The forms derived in the previous sections were based on a two-body Hamiltonian. However, interactions derived from first principles contain at least three-body forces [31], which are crucial for performing *ab initio* calculations with some predictive power. In a similar manner, the more phenomenological EDF-based methods must include terms of higher order than a two-body interaction, which is usually done by the inclusion in the EDF of terms with density dependencies. In particular, the

[1] This assumption, however, cannot be expected to be valid for all nuclei. Each nucleus enters the expression for δV_{pn} for four different nuclei, such that ultimately *all* nuclei had to have the same mean field for this assumption to be fulfilled.

saturation of nuclear matter cannot be satisfactorily described without taking into account these terms [32].

A three-body force adds a term $\frac{1}{36}\sum_{i,j,k,l,m,n} v_{ijklmn}\, a_i^\dagger a_j^\dagger a_k^\dagger a_n a_m a_l$ to the Hamiltonian (2). In the HF approximation, its contribution to the binding energy is given by

$$\begin{aligned} E_{3b}^{\mathrm{HF}}(N,Z) &= \frac{1}{6}\sum_{n,n',n''=1}^{N} \bar{v}^{N,Z}_{nn'n''nn'n''} + \frac{1}{2}\sum_{n,n'=1}^{N}\sum_{p=1}^{Z} \bar{v}^{N,Z}_{nn'pnn'p} \\ &+ \frac{1}{2}\sum_{n=1}^{N}\sum_{p,p'=1}^{Z} \bar{v}^{N,Z}_{npp'np''} + \frac{1}{6}\sum_{p,p',p''=1}^{Z} \bar{v}^{N,Z}_{pp'p''pp'p''}\,, \end{aligned} \tag{8}$$

using a notation analogous to that of Eq. (3). In the frozen HF approximation, a Hamiltonian including two-body and three-body forces leads to

$$\begin{aligned} \delta V_{pn}^{\mathrm{HF_{frozen}}}(N,Z) &= -\frac{1}{4}\Bigg[\sum_{n=N-1}^{N}\sum_{p=Z-1}^{Z} \bar{v}_{npnp} + \frac{1}{2}\sum_{n,n'=N-1}^{N}\sum_{p=Z-1}^{Z} \bar{v}_{nn'pnn'p} \\ &+ \frac{1}{2}\sum_{n=N-1}^{N}\sum_{p,p'=Z-1}^{Z} \bar{v}_{npp'npp'} + \sum_{n=1}^{N-2}\sum_{n'=N-1}^{N}\sum_{p=Z-1}^{Z} \bar{v}_{nn'pnn'p} \\ &+ \sum_{p=1}^{Z-2}\sum_{n=N-1}^{N}\sum_{p'=Z}^{Z-2} \bar{v}_{npp'n'p'}\Bigg]. \end{aligned} \tag{9}$$

The first three lines represent the two-body and three-body interactions between the last two neutrons and the last two protons. The last two lines of Eq. (9), however, contain a sum over all other nucleons, which is incompatible with the interpretation of $\delta V_{pn}(N,Z)$ as the interaction between the last two neutrons and protons.

Most energy density functionals constructed for self-consistent mean-field calculations include a nonlinear density-dependent two-body term of the form $\frac{1}{4}\sum_{i,j,m,n} v_{ijkl}\, f(\rho_n+\rho_p)\, a_i^\dagger a_j^\dagger a_n a_m$, where ρ_n and ρ_p are the local densities of neutrons and protons. Popular examples for $f(\rho_n+\rho_p)$ range from the simple noninteger powers of the total density $f(x)=x^\alpha$, such as that used with most Skyrme and Gogny interactions, to the very elaborate density dependencies $f(x)\sim[1+b(x+d)^2]/[1+c(x+d)^2]$ used in modern density-dependent relativistic mean-field models [33,34]. Any density dependence that is not a simple polynomial of the total density gives rise to δV_{pn} values that cannot be separated into neutron and proton contributions, even within the frozen HF approximation.

We will not give explicit expressions for the HFB case with three-body forces or density-dependent terms. It should be obvious by now that even making the assumption of a frozen common canonical basis will lead to a lengthy and complicated expression for $\delta V_{pn}(N,Z)$ that does not allow for an intuitive interpretation.

D. Discussion

Even when making the drastic approximation that the four nuclei entering the calculation of $\delta V_{pn}(N,Z)$ can be described by the same mean field, the expression that is obtained for realistic models includes a summation over all single-particle levels.[2] Furthermore, the occupation of the levels around the Fermi energy is affected by the addition or the removal of nucleons, and the contribution of each single-particle level to $\delta V_{pn}^{\mathrm{HFB_{frozen}}}(N,Z)$ is weighted with the difference of its occupation between the nuclei. It is therefore doubtful that δV_{pn} allows us to isolate an empirical interaction between the last neutron and proton orbitals, as claimed in Ref. [22].

Moreover, one might wonder whether the approximation of a frozen canonical basis necessary to derive Eqs. (5) and (7) is ever satisfied. To change the number of neutrons or protons by two induces rearrangement and polarization effects that modify the single-particle wave functions for both kinds of nucleons. Even if these effects are most often small, it should not be forgotten that $\delta V_{pn}(N,Z)$ is a tiny fraction of the total binding energy only, ranging from 10^{-2} in light nuclei to 10^{-5} in heavy ones. Therefore, even small rearrangement effects can have a large impact on the values obtained for $\delta V_{pn}(N,Z)$. We will analyze the validity of the frozen basis assumption for a few selected cases in Sec. IV C. Finally, a self-consistent mean-field description of a nucleus provides a reasonable first approximation, but it neglects correlations beyond the mean field that also contribute to the binding energy on the MeV scale [35,36]. These correlations cannot be cast in a simple form involving only the interaction between a few particles, and they also destroy the simple relation between δV_{pn} and proton-neutron matrix elements.

In the remaining part of this article, we investigate the importance of self-consistency, deformation, pairing, and configuration mixing for the description of data for δV_{pn}. We also analyze to what extent δV_{pn} values can be identified with the effective proton-neutron interaction.

III. THE MODELS

A. The beyond-mean-field model

Our method used to calculate binding energies for the ground states of even-even nuclei is described in detail in Refs. [35,36]. In our analysis, we use the energies as tabulated in [37], and we add a few nuclei in the vicinity of ^{208}Pb. As effective interaction, we employ the SLy4 parametrization of the Skyrme energy density functional [38] for the mean-field channel in connection with a density-dependent zero-range pairing interaction.

Starting from a set of mean-field calculations including a constraint on the axial quadrupole moment, two kinds of correlations beyond the mean field are introduced. First, the deformed wave functions are projected on both fixed particle numbers and on angular momentum $J=0$. In a

[2] A similar observation has been made by Van Isacker *et al.* [27], who state that "$\delta V_{pn}(N,Z)$ is an average np interaction over the last few nucleons," but without giving any reference.

collective model terminology, these correlations would be called rotational correlations. A second step of our method consists in the mixing of projected wave functions with different intrinsic axial quadrupole moments of the underlying mean-field state in a generator coordinate method (GCM). In the language of collective models, this corresponds to a vibrational correction. The final wave function has the form

$$|JM\nu\rangle = \sum_q f_{J,\nu}(q)\hat{P}^J_{M0}\hat{P}_N\hat{P}_Z|q\rangle\,. \tag{10}$$

The ket $|q\rangle$ is a (paired) self-consistent mean-field state of axial quadrupole deformation q. The operators $\hat{P}_N$, $\hat{P}_Z$, and $\hat{P}^J_{M0}$ project out the component with the particle numbers and angular momentum quantum number we are interested in. The weights $f_{J,\nu}(q)$ defining the mixing of the projected wave functions with respect to q are obtained by variation of the total energy.

We stress that there are no assumptions made in the model about the amplitude of the quadrupole fluctuations introduced into the calculations. Depending on the structure of a nucleus, this amplitude either corresponds to a small vibration around a pronounced minimum, to a large-amplitude motion in a soft and wide potential well, or to the mixing of several states around coexisting minima in the deformation energy surface.

In the following, we will compare results obtained from the energies determined using three wave functions that successively add quadrupole correlations: (1) self-consistent spherical mean-field states $|q = 0\rangle$, (2) the self-consistent mean-field minimum in the space of axial reflection-symmetric deformations $|q_{\min}\rangle$, which might be spherical, and (3) the ground state obtained after configuration mixing of $J = 0$ projected axial quadrupole. We refer to these wave functions in the following as projected GCM. The energy gained through these correlations will be called beyond-mean-field correlation energy in what follows. In each of these cases, the wave functions are projected on particle number.

B. Liquid-drop model

The Strutinsky theorem [39,40] allows us to decompose the binding energy into a "macroscopic" liquid-drop part and a microscopic "shell correction." In this picture, the macroscopic energy defined through the liquid-drop model varies smoothly with N and Z, without any correlation energies from deformation, shell effects, or fluctuations in collective degrees of freedom. It constitutes a reference with respect to which one can put into evidence all quantum effects.

In the figures below we show macroscopic energies calculated from a liquid-drop model whose parameters have been adjusted to reproduce the average binding energies of spherical nuclei calculated with the Skyrme interaction SLy4 [10]. In addition to the standard volume, volume symmetry, surface, and (direct) Coulomb terms, the macroscopic model comprises surface symmetry, curvature, and Coulomb exchange terms:

$$\begin{aligned} E_{\rm mac}(N,Z) &= (a_{\rm vol}+a_{\rm sym}\,I^2)A + (a_{\rm surf}+a_{\rm surf,sym}\,I^2)A^{2/3} + a_{\rm surf}A^{1/3} \\ &\quad + \frac{3}{5}\frac{Z^2e^2}{r_0A^{1/3}} - \frac{3}{4}\left(\frac{3}{2\pi}\right)^{2/3}\frac{Z^{4/3}e^2}{r_0A^{1/3}}, \end{aligned} \tag{11}$$

where $A = N + Z$ and $I = \frac{N-Z}{N+Z}$. The radius constant r_0 entering the Coulomb energies is determined from the nuclear matter saturation density ρ_0 of SLy4 as $r_0^3 = 3/(4\pi\rho_0)$.

The dominating contribution to δV_{pn} by far comes from the volume and surface symmetry energies [24]:

$$\delta V_{pn} \approx 2(a_{\rm sym} + a_{\rm surf,sym}A^{-1/3})\,A^{-1}\,. \tag{12}$$

The global A^{-1} scaling factor in this expression originates from the denominator of the $I^2\,A = \frac{(N-Z)^2}{N+Z}$ factor in the symmetry and surface symmetry energy terms, which do not cancel out in δV_{pn}.

There are two contributions to this term that have the same scaling [41]: the first one is the difference in kinetic energy between protons and neutrons that fill separate potential wells, and the other is the isovector part of the nucleon-nucleon interaction. The latter has a shorter range than the average distance between nucleons, such that in a semiclassical approximation it acts between nearest neighbors only, leading to the characteristic A and $A^{1/3}$ scaling of terms in Eq. (12). The contribution of all other terms in Eq. (11) to δV_{pn} is not exactly zero, but it is too small to be resolved in the plots shown below. A standard liquid-drop model obtained with a "best fit" to experimental masses gives δV_{pn} values that are systematically larger than those obtained from Eq. (11), mainly because the volume symmetry coefficient $a_{\rm sym}$ has a slightly larger value than the one determined from the SLy4 interaction.

IV. RESULTS

A. Global behavior of δV_{pn}

The binding energies of Refs. [35,36] and tabulated in [37] cover the region of even-even nuclei heavier than ^{16}O for which experimental data are available plus a few additional nuclei around doubly magic systems. For the present study, we calculated a few extra nuclei around ^{208}Pb. Values obtained for δV_{pn} with this sample of nuclei are plotted as maps in Fig. 1. For a better resolution of the local fluctuations, the same data are plotted for isotopic chains as a function of the number of neutrons in Fig. 2 and for isotonic chains as a function of proton number in Fig. 3.

The spherical macroscopic values are given each time in Figs. 1(a)–3(a). All nuclei between the drip lines are represented for the LDM results in Fig. 1, whereas in Figs. 2 and 3 results are restricted to the same set of nuclei shown in the other panels. The macroscopic δV_{pn} values exhibit a regular smooth pattern and fall off with $\sim 1/A$. The slope of the decrease is related to the symmetry and surface symmetry energy coefficients of the EDF, Eq. (12). This smooth systematic decrease of the δV_{pn} values with increasing A has been sometimes interpreted as a result of "the gradual decrease in valence proton and neutron orbital overlaps due to the occupancy of shells of different average radii" [19,22]. This is, at best, a model-dependent statement that cannot be translated to methods that calculate the energy from the interaction between all occupied particles. In particular, at no point in the derivation of the LDM expression (12) does one

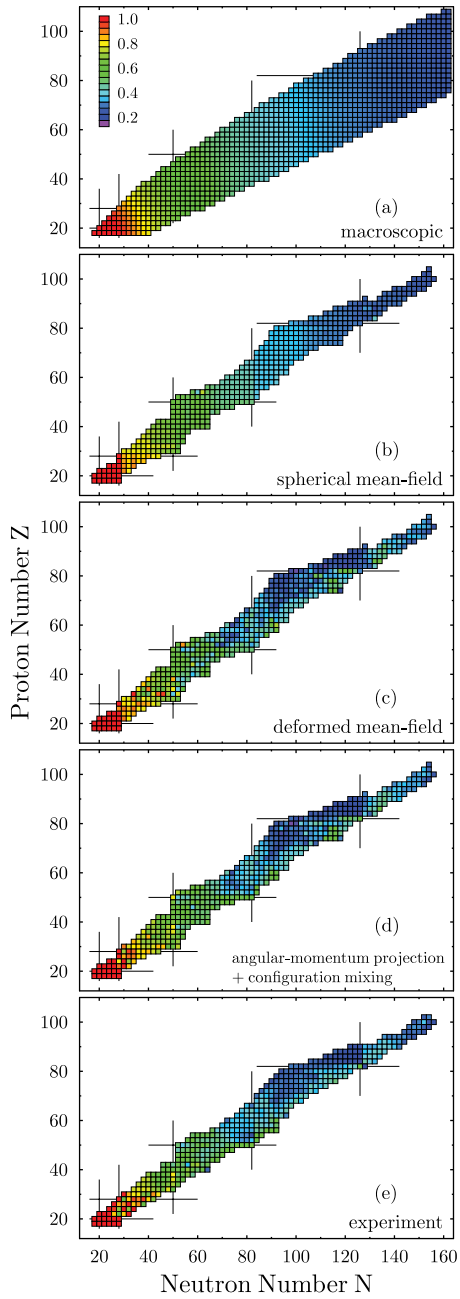

FIG. 1. (Color online) Maps of δV_{pn}: (a) calculated with a spherical liquid-drop formula having the average properties of the SLy4 interaction, (b) by self-consistent calculations with SLy4 obtained assuming spherical nuclei, (c) allowing for (axially) deformed shapes, and (d) derived from $J = 0$ projected configuration mixing calculations. (e) The experimental data.

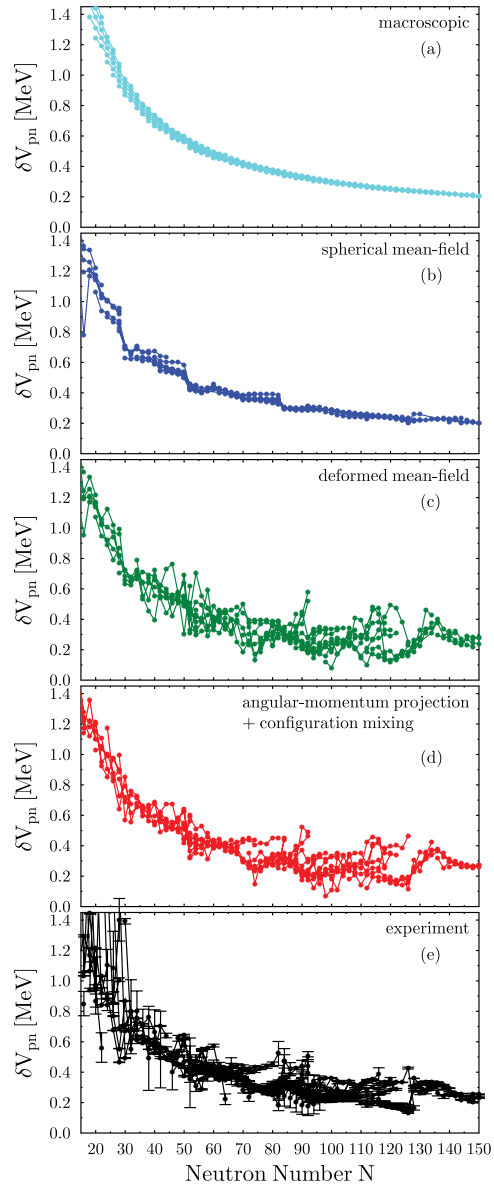

FIG. 2. (Color online) Same data as in Fig. 1, but plotted for isotopic chains as a function of neutron number.

have to consider the form of the single-particle wave functions and their overlaps. Instead, it is only assumed that all occupied single-particle wave functions add up to the saturation density inside the nucleus.

The smooth trend of the macroscopic calculation is still apparent in the spherical self-consistent mean-field results. Some deviations appear, however, which are related to the magic numbers at 20, 28, 50, 82, and 126. For nuclides just below these shell closures, the spherical mean-field results are slightly larger than the LDM ones, whereas they take slightly smaller values for nuclei just above. As a consequence, δV_{pn} values do not fall off continuously with A but form sheets separated by the shell closures.

Relaxing the constraint of spherical symmetry strongly modifies the behavior of δV_{pn} by giving rise to rapid fluctuations around the smooth trend, with an amplitude of up to 200 keV. This change can be directly related to the effect of deformations on binding energies. The variations of quadrupole deformation and of the associated energy gain with N and Z over the entire nuclear chart have been presented in Figs. 9 and 16 of Ref. [36]. The energy gain due to deformation can reach more than 20 MeV and can vary rapidly from one nucleus to the other. Any mismatch in the evolution of

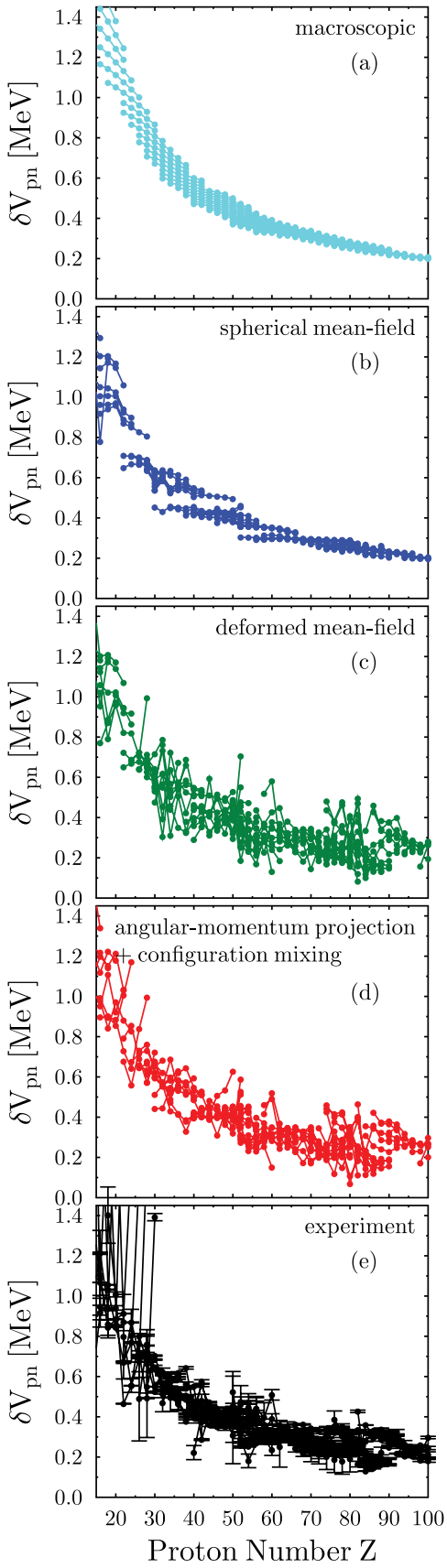

FIG. 3. (Color online) Same data as in Fig. 1, but plotted for isotonic chains as a function of proton number.

deformation energy between the four nuclei entering δV_{pn} can dramatically change its value.

To illustrate the impact of deformation and correlations on δV_{pn}, the quadrupole deformation β_2, deformation, and correlation energies for nuclei heavier than ^{132}Sn are presented in Fig. 4. As expected, the absolute value of the deformation energy increases slowly at first when moving away from the proton and neutron shell closures and then more rapidly until it peaks at almost 18 MeV in the rare-earth region and above 20 MeV for actinides. As indicated in the inset in Fig. 4(d), δV_{pn} is defined as the sum of the energies of the nuclei on the diagonal minus the sum of the energies of the nuclei on the antidiagonal. Figure 4 gives an intuitive illustration of how the deformation and beyond-mean-field correlation energies contribute to δV_{pn}. Along a line going from ^{132}Sn to ^{208}Pb and beyond, the deformation energy varies rapidly and nonlinearly and brings a very large contribution to $\delta V_{pn}(N, Z)$. On the contrary, for nuclei located close to a spherical shell closure for one nucleon species and midshell for the other, the lines of equal deformation and correlation energy are nearly parallel to the N or Z axis, leading to a pairwise cancellation of similar deformation energies. The fine structure of this cancellation depends, of course, on the deformed shell structure of the four nuclei entering a given $\delta V_{pn}(N, Z)$ value and leads to an erratic behavior of δV_{pn}, particularly visible when drawn for isotopic or isotonic chains, as in Figs. 2 and 3. The same behavior is also seen in the experimental data. It is worthwhile to mention that there is no direct relation between the size of the deformation and the deformation energy or between the sign of the deformation, prolate, or oblate and the deformation energy. In particular, the transition between oblate and prolate shapes in a region of shape coexistence around the neutron-deficient Pb isotopes does not leave obvious traces in the ground-state deformation energy and, hence, in the calculated δV_{pn} values. As one may expect, introducing beyond-mean-field correlations evens out the effect of static deformation. The effect of configuration mixing is, indeed, a spreading of the ground-state wave function around the mean-field minimum and a mixing of coexisting shapes. The beyond-mean-field correlation energy varies rapidly only around shell closures and has its largest impact on the $\delta V_{pn}(N, Z)$ values in these regions. We will analyze its impact in more detail for selected nuclei below.

The very rapidly varying behavior of δV_{pn} around the $N = Z$ line that sticks out in the experimental data for light nuclei in Figs. 1, 2, and 3 is not reproduced by any of our calculations. This anomaly is due to the Wigner energy [27,28,42,43], whose origin is not described by present-day EDF models; see Refs. [28,44] for further discussion of this deficiency.

In the literature one cannot find, however, a unique definition of the Wigner energy. Sometimes this notion is used for an anomalous additional contribution to the binding energy of the $T = 0 \Leftrightarrow N = Z$ member of an isobaric multiplet compared to the $(N - Z)^2$ extrapolation from the other isobars [45], but more often the Wigner energy denotes a contribution to the binding energy that is linear in $|T_z| = |N - Z|$. Such a term arises, for example, from a Hamiltonian that is invariant under Wigner's SU(4) symmetry, $E \sim T(T + 4) = E_{\text{sym}} + E_{\text{Wigner}}$.

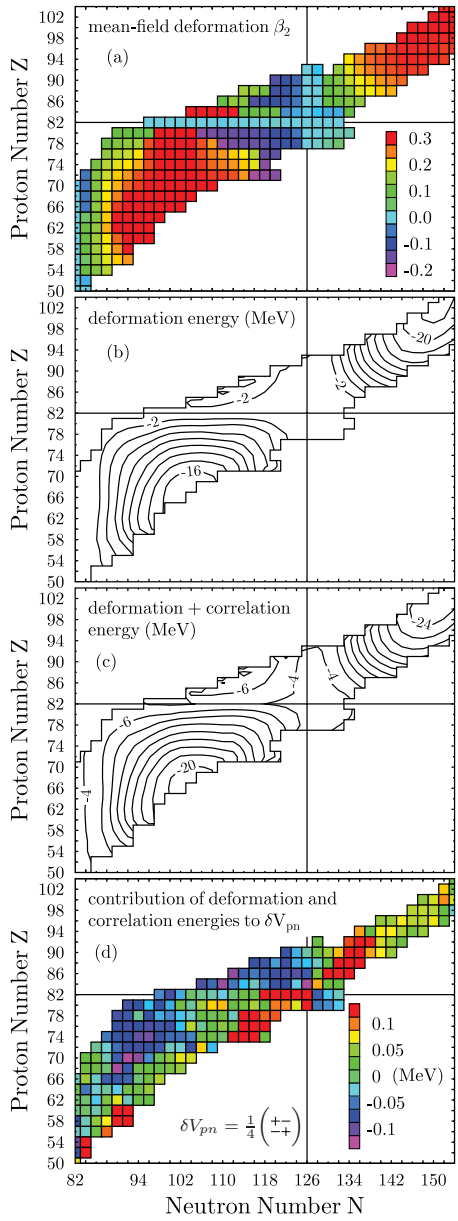

FIG. 4. (Color online) Effect of deformation and correlation energies on δV_{pn} values for heavy nuclei. (a) Map of the dimensionless quadrupole deformation β_2 of the mean-field ground state, (b) contour plot of the static deformation energy, (c) contour plot of the sum of the static deformation and dynamical beyond-mean-field correlation energies, and (d) map of the contribution of deformation and dynamical correlation energy to δV_{pn}. The total δV_{pn} value is then obtained by adding the spherical mean-field value. The inset gives a reminder of the relative signs of the four contributions to δV_{pn}, with their distance being drawn on the same scale as the one used in the contour plot.

When using this second concept of a Wigner energy, the anomaly of binding energies at $N = Z$ is the consequence of the Wigner energy E_{Wigner} having a discontinuity in its derivative at $T_z = 0$ and not of an additional binding of $N = Z$ nuclei. There are many reasons why Wigner's SU(4) symmetry is not realized in nuclei [27,28,42,43,46], which suppresses the linear term in $|N - Z|$ compared to the quadratic one. Still, traces of such a linear term are implicitly contained in all realistic shell-model calculations [28,42,45,47] and explicitly in the Duflo-Zuker mass formula [5]. It is noteworthy that the macroscopic-microscopic mass models [6] and the Skyrme-HFB mass formulae [7] also contain explicit phenomenological corrections for the Wigner energy that, in fact, combine both of the concepts of Wigner energy mentioned above; see also the discussion in Ref. [1]. Several mass differences have been put forward as indicators or even measures of the Wigner energy, most prominently double-β-decay Q values [42,43] or a difference between three different δV_{pn} values [28]. It has to be stressed, however, that δV_{pn} itself is not a measure of the Wigner energy.

B. Selected chains of nuclei

1. *Isotopic chains of magic nuclei*

To demonstrate how δV_{pn} is built up from different types of correlations, let us examine now its evolution along cuts through the N-Z plane. We first look at the two isotopic chains of Sn and Pb, corresponding to closed proton shells, in Figs. 5 and 6. We showed in Ref. [14] for the $Z = 50$ Sn isotopic chain that static deformation and dynamical correlation energies are key ingredients in reproducing the two-proton separation energies across the $Z = 50$ shell and in explaining in an intuitive way the mutually enhanced magicity around ^{132}Sn.

The results for Sn isotopes are displayed in Fig. 5 and those for Pb in Fig. 6. The dimensionless deformation parameter β_2^{calc} is related to the intrinsic mass quadrupole moment of the self-consistent mean-field wave functions $\langle q|(2z^2 - x^2 - y^2)|q\rangle$ as

$$\beta_2^{\text{calc}} \equiv \sqrt{\frac{5}{16\pi}}\,\frac{4\pi}{3R_0^2 A}\langle q|(2z^2 - x^2 - y^2)|q\rangle, \qquad (13)$$

with $R_0 \equiv 1.2\,A^{1/3}$ fm. In Figs. 5(a)–5(c) and 6(a)–6(c), the results for isotopic chains with two protons less are also displayed, such that the values for all four nuclei entering δV_{pn} are given in the same plot. The contribution of deformation and correlation energy to a given $\delta V_{pn}(N, Z)$ value can be extracted from the plot by first taking the difference between the energies for N and $N - 2$ on the curves for Z and $Z - 2$, and then subtracting the value for $Z - 2$ from the one for Z. To facilitate this comparison, the deformation and correlation energies have been multiplied by a factor of 1/4, so that the quantity entering δV_{pn}, Eq. (1), is plotted on the figure. The magnitude of the contributions of deformation and correlations to $\delta V_{pn}(Z, N)$ is directly related to the difference in slopes of the curves for Z or $Z - 2$ for a given N. The largest contributions are obtained when one of the slopes is much steeper than the other.

The ground-state configurations obtained for most Sn and Pb isotopes are spherical; some midshell isotopes are slightly deformed. However, the energy gain due to deformation in those cases is small, smaller than 200 keV, and it originates from a deformed minimum nearly degenerate with the spherical configuration. In contrast, the deformation and gain in deformation energy for the ground states of the nonmagic

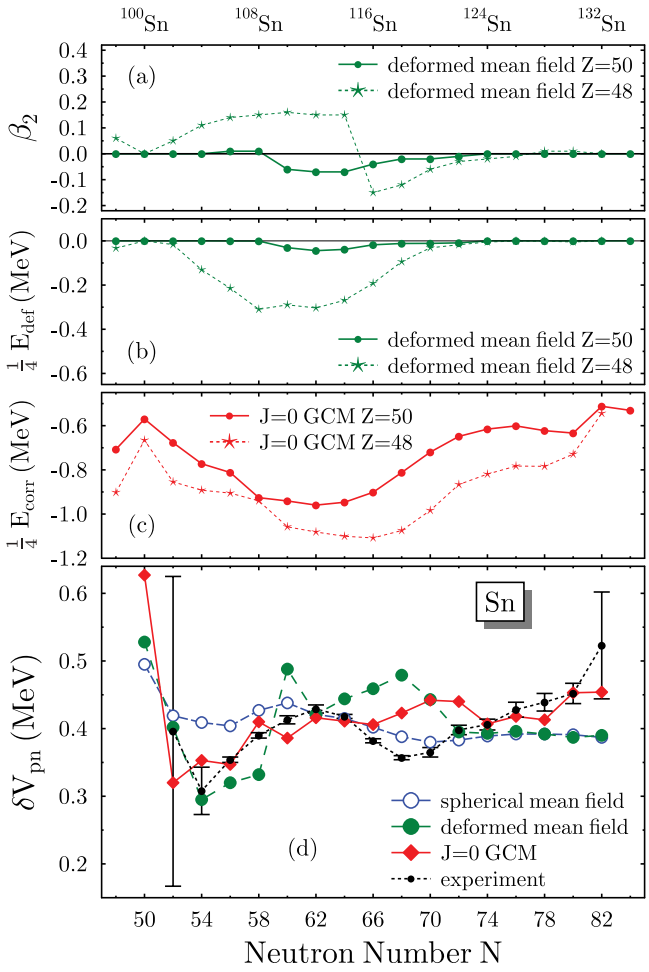

FIG. 5. (Color online) (a) Intrinsic deformation of the mean-field ground state, (b) 1/4 of the deformation energy, (c) 1/4 of the beyond-mean-field correlation energy, and (d) δV_{pn} values obtained from spherical mean-field calculations, deformed mean-field calculations, $J = 0$ projected GCM calculations, and experimental data for the chain of Sn ($Z = 50$) isotopes. For the deformation, deformation energy, and correlation energy the values for Cd ($Z = 48$) isotopes are also shown.

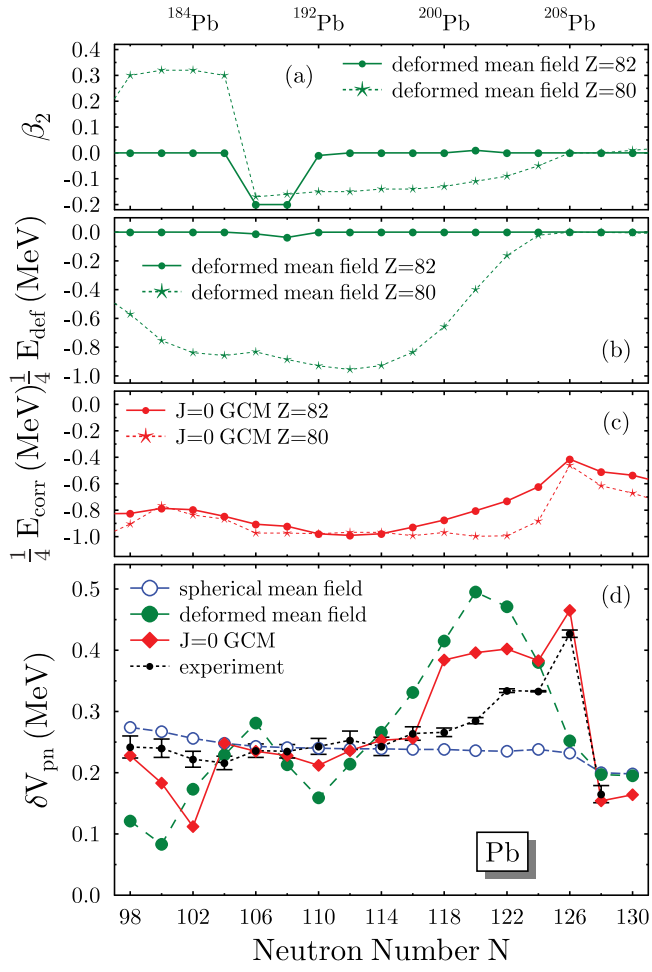

FIG. 6. (Color online) The same as Fig. 5, but for the chain of Pb ($Z = 82$) isotopes. The oblate ground-state deformation found for Hg isotopes is confirmed by experiment below $N = 122$.

$Z - 2$ isotopic chains can be large and vary rapidly for some neutron numbers. For those cases, the contribution of the deformation energy to δV_{pn} is large. This clearly indicates that one cannot assume to describe all four nuclei entering δV_{pn} by a common mean field, even for closed-shell nuclei.

The correlation energy is larger for all Cd and Hg isotopes than for Sn and Pb nuclei with the same N. However, the slopes of the Z and $Z - 2$ curves differ significantly for a few isotopes only, and its contribution to δV_{pn} is large only for these neutron numbers. Nevertheless, the beyond-mean-field correlations level out the rapidly fluctuating effect of static deformations. Their contribution to the binding energy also plays a key role in the description of the two-proton separation energies across the $Z = 50$ and $Z = 82$ shells [14,36].

The agreement between the experimental data and the results of the beyond-mean-field calculation is very satisfactory for the Sn and Pb isotopic chains, as can be seen in Figs. 5(d) and 6(d). In particular, only the latter calculation is able to describe the rise of δV_{pn} up to $N = 126$ and its sudden drop beyond. The rapid variation of δV_{pn} around ^{132}Sn and ^{208}Pb is mainly due to the onset of substantial beyond-mean-field correlations around doubly magic nuclei. This scenario is much more involved than the proton-neutron interaction between the valence orbitals invoked in Ref. [48]. A detailed analysis of the contributions to the δV_{pn} value of ^{208}Pb is given in Sec. IV C.

2. *Onset of deformation in rare-earth nuclei*

Let us now analyze the isotopic chains of Ba ($Z = 56$), Nd ($Z = 60$), and Gd ($Z = 64$), which cover a region of nuclei with a large variation of deformation on both sides of the spherical $N = 82$ shell closure. Results of our calculations are compared with the experimental data in Figs. 7, 8, and 9. Intrinsic deformations calculated with Eq. (13) are compared to values taken from Refs. [49,50] that are determined from experimental $B(E2)$ values making the assumption of a rigid axial rotor

$$\beta_2^{\text{expt}} \equiv \frac{4\pi}{3ZR_0^2}[B(E2, 0_1^+ \to 2_1^+)]^{1/2}, \qquad (14)$$

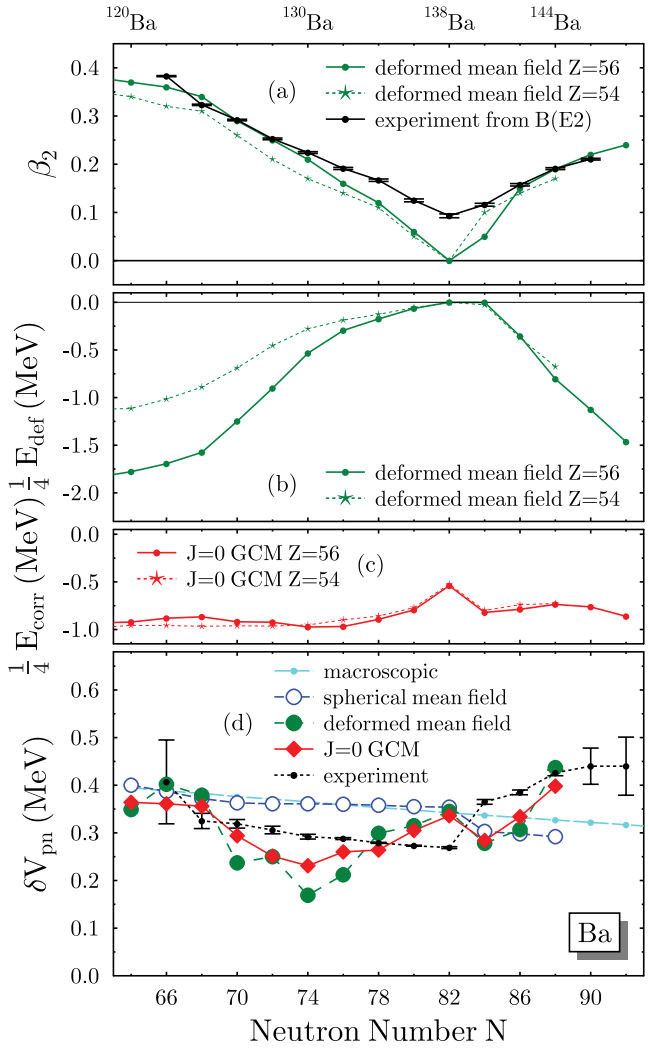

FIG. 7. (Color online) (a) Intrinsic deformation of the mean-field ground state compared with experimental data taken from [50], (b) 1/4 of the deformation energy, (c) 1/4 of the beyond-mean-field correlation energy, and (d) δV_{pn} values obtained from the macroscopic model, spherical mean-field calculations, deformed mean-field calculations, $J = 0$ projected GCM calculations, and experimental data for the chain of Ba ($Z = 56$) isotopes. For the deformation, deformation energy, and correlation energy the values for Xe ($Z = 54$) isotopes are shown as well (see text).

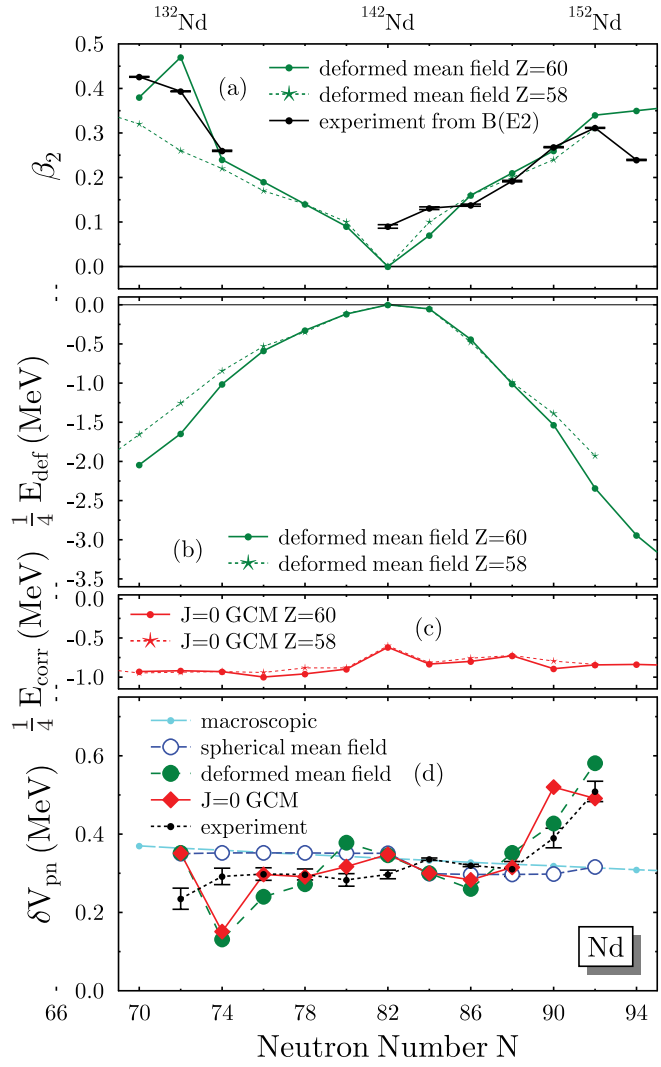

FIG. 8. (Color online) The same as Fig. 7, but for the chain of Nd ($Z = 60$) isotopes.

with $R_0 \equiv 1.2\,A^{1/3}$ fm. For well-deformed nuclei, theoretical (13) and experimental (14) values are in excellent agreement. Around spherical shell closures, however, the lowest 2^+ state is dominated either by noncollective two-quasiparticle configurations or by fluctuations in collective degrees of freedom, neither of which can be described by the mean-field ground state.

The spherical mean-field result for δV_{pn} does not show any structure these three isotopic chains except for a tiny drop at the $N = 82$ shell closure that becomes rapidly smaller with increasing proton number. Besides that, the spherical mean-field values remain very close to the macroscopic ones for all three chains of nuclei. The only isotopes to remain spherical when deformations are allowed are those with $N = 82$. All heavier isotopes are prolate, with a very similar variation of deformation as a function of N for all three isotopic chains. Lighter isotopes are prolate for Ba and Nd and oblate for Gd. Although the deformation varies with N in a rather similar way for the three chains, the effects of deformation and beyond-mean-field correlations on δV_{pn} are different. Deformation and correlations do not bring very large contributions, but they induce a significant change of behavior of δV_{pn} for Ba and Nd. Note also that the changes with respect to the spherical case bring theory closer to experiment with very few exceptions. The contribution from deformation energy overcorrects the spherical result for δV_{pn}, in particular by making δV_{pn} smaller below $N = 82$ and larger above that value. The beyond-mean-field correlations straighten the curve and bring it very close to the data.

Comparing the three isotopic chains, the largest deviation between the experimental and the macroscopic δV_{pn} values is observed for the Ba ($Z = 56$) isotopes. For the isotopes below $N = 82$ (with the possible exception of the lightest one, $N = 66$), the experimental values are smaller, whereas above

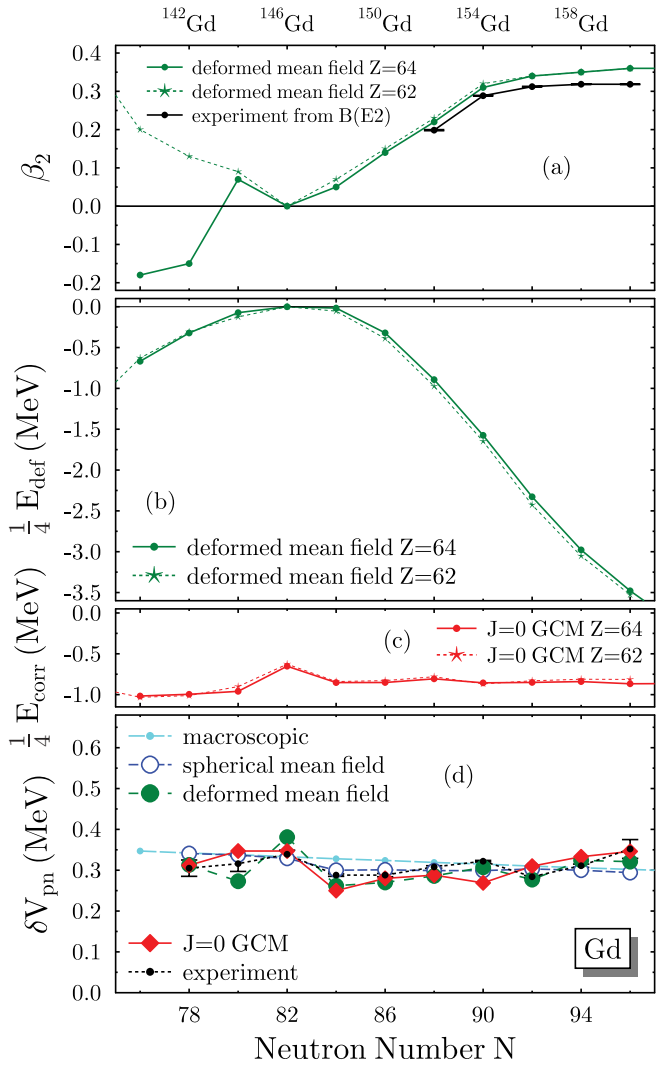

FIG. 9. (Color online) The same as Fig. 7, but for the chain of Gd ($Z = 64$) isotopes.

$N = 82$ they are larger. The same overall behavior is also found for Nd ($Z = 60$), but with a smaller deviation from the macroscopic results. For Gd ($Z = 64$), the experimental data lie almost on a straight line, very close to the macroscopic results.

The EDF models provide a simple explanation of these different behaviors. The three chains present a similar evolution as a function of N, going from deformed to spherical to deformed shapes again. However, looking at Fig. 4, one can see that the chains are located differently with respect to the center of the deformed region. The Ba ($Z = 56$) isotopes are situated at the lower end, where the deformation energy grows with N at a very different rate for Z and $Z - 2$ and brings a large contribution to δV_{pn}. The Gd ($Z = 64$) chain is close to the center of the deformed region where the deformation energy of adjacent isotones grows synchronously. The δV_{pn} values are unaffected by deformation in the Gd isotopes, and it is also remarkable that the shape transition from a prolate shape for $Z = 62$ to an oblate one for $Z = 64$ at $N = 78$ does not visibly affect the δV_{pn} value obtained from the deformed mean-field calculation. These examples indicate that δV_{pn} cannot always be expected to be a sensitive indicator for changes in deformation.

3. δV_{pn} along lines of constant $N + Z$ or $N - Z$

Let us now examine the evolution of δV_{pn} along other cuts through the chart of nuclei. In Fig. 10, results for nuclei on a line of constant $T_z = N - Z = 32$ are provided as a function of $A = N + Z$. Available data start at the doubly magic nucleus ^{132}Sn, cover the entire rare-earth region, and extend beyond $Z = 82$. Most of the nuclei along this chain are deformed, except for $Z = 50$ and 82. The deformation energy takes its largest absolute value of around 16.8 MeV for ^{168}Er at $Z = 68$. However, it is not the magnitude of the deformation energy that governs the size of its contribution to

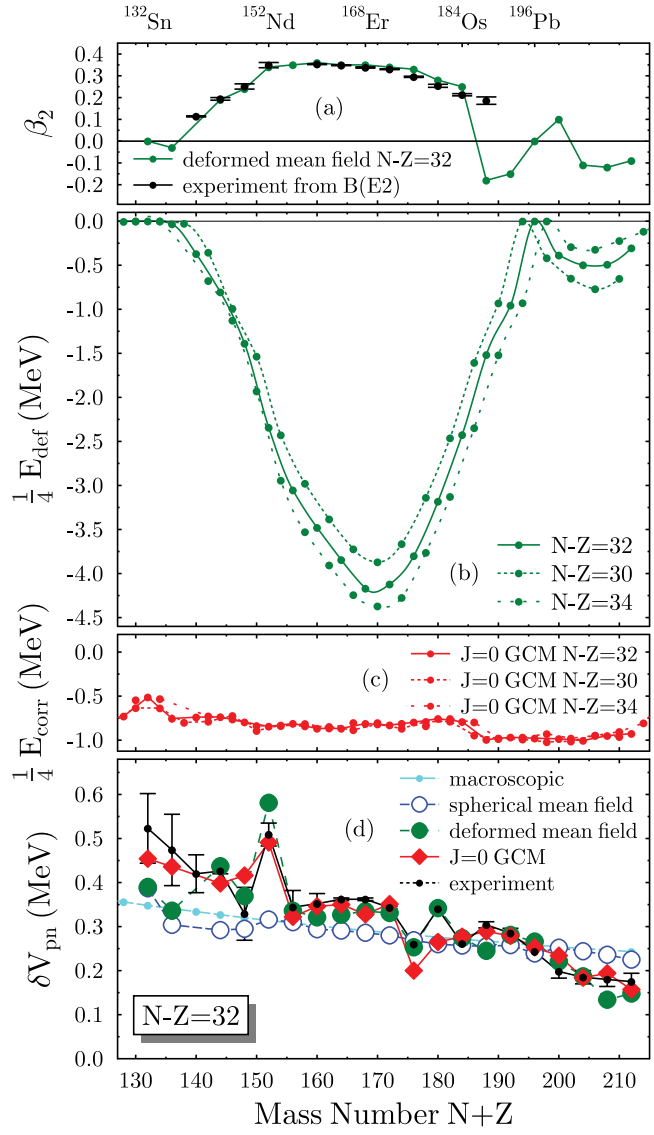

FIG. 10. (Color online) The same as Fig. 7, but for the chain of constant $N - Z = 32$. The nuclei for which data exist are expected to be prolate, whereas the systematics of rotational bands and radii in the Hg isotopic chain suggests that ^{194}Hg is oblate in its ground state, in agreement with the calculation.

δV_{pn} but how the curve for $T_z = 32$ diverges from those for $T_z = 30$ and 34. Indeed, the contribution of the deformation energy to δV_{pn} is obtained as the sum of the energies of two successive points on the $T_z = 32$ line from which one subtracts the sum of the values on the $T_z = 30$ and $T_z = 34$ lines corresponding to the intermediate A value. The contributions of deformation and beyond-mean-field correlations reinforce themselves for the lightest nuclei, leading to a rather irregular pattern, significantly different from the structureless spherical results. It is remarkable that δV_{pn} values obtained from the beyond-mean-field calculation follow very closely the many irregularities of the experimental data.

Results obtained for two nuclear chains corresponding to fixed values of A, which are perpendicular to the $N - Z = 32$ chain, are plotted in Fig. 11. The first one corresponds to $A = 132$ and extends from the very deformed neutron-deficient ^{132}Nd to the doubly magic ^{132}Sn. As in the case of the Ba and Nd isotopic chains, the different onset of deformation and correlation energy for Z and $Z - 2$ lowers δV_{pn} relative to the macroscopic values below the $N = 82$ shell closure, whereas it is enhanced for ^{132}Sn. Note for this nucleus the significant differences between the deformed and the beyond-mean-field calculations. The change of behavior for $N - Z = 32$ of δV_{pn} with respect to the spherical and macroscopic values is very nicely described by the beyond-mean-field calculation.

The second isobaric chain in Fig. 11, $A = 168$, almost follows the diagonal in Fig. 4. All isobars are deformed, and the deformation increases gradually when going from the very neutron-deficient ^{168}Pt to ^{168}Er, a nucleus located in the center of the deformed rare-earth region. The deformed mean-field and beyond-mean-field calculations give very similar δV_{pn} values and agree well with the data. For the lighter isobars, the δV_{pn} values are smaller than the macroscopic ones, whereas for ^{168}Er they suddenly increase to values above them. For the chains that we discussed up to now, the sudden increase of δV_{pn} from below to above macroscopic values took place when crossing a spherical shell closure, i.e., with decreasing deformation. In the case of the $A = 168$ chain, the sudden increase of δV_{pn} has its origin in the saturation of deformation energy with increasing asymmetry.

Again, the deviation of δV_{pn} from the macroscopic value depends on the difference of increase in deformation energy in adjacent nuclei.

4. *Doubly magic nuclei and mutually enhanced magicity*

In Figs. 5, 10, and 11, the δV_{pn} value of ^{132}Sn sticks out as being larger than that of all surrounding nuclei. The same result is obtained for ^{208}Pb. In both cases, these δV_{pn} values are also much larger than the macroscopic trend. A similar singular behavior for doubly magic nuclei is also found with other mass filters, such as two-particle separation energies or Q_α values: the value obtained for a doubly magic nucleus is much larger than those of adjacent nuclei, including the semimagic ones. This gives the impression that the shell closure of one nucleon species reinforces the magicity of the other, an effect sometimes called "mutually enhanced magicity" in the literature [1,51,52]. This effect is not described by pure mean-field models for which two-nucleon separation

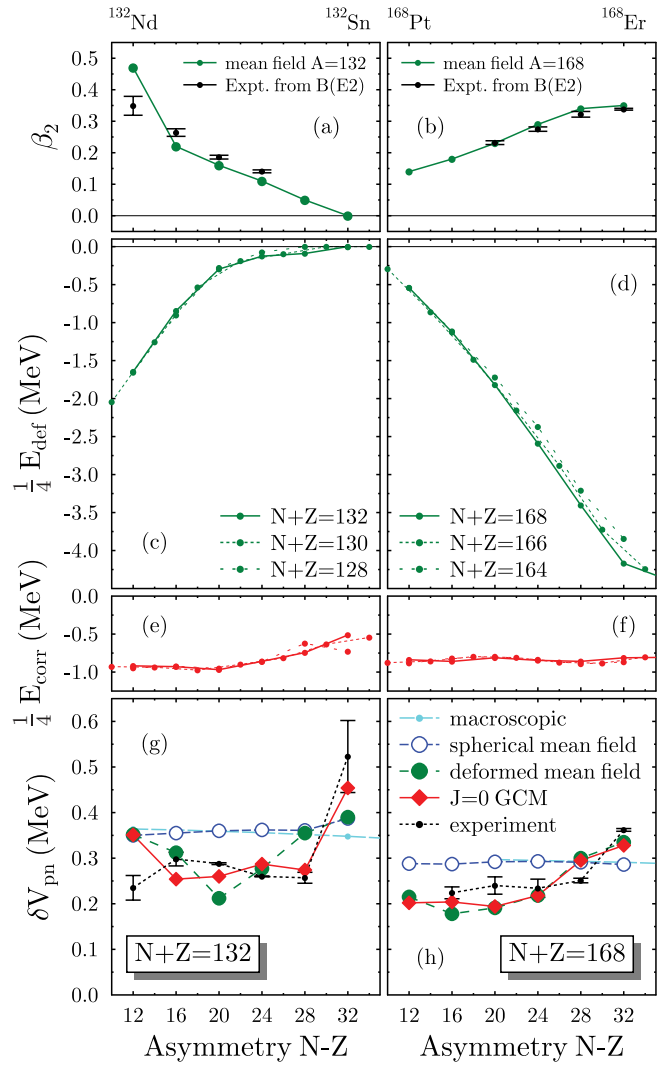

FIG. 11. (Color online) The same as Fig. 7, but for the isobaric chains with $A = N + Z = 132$ and $A = 168$.

energies or Q_α values across a shell closure usually show very little variation with the number of particles of the other species, in stark contrast to the data. In Refs. [14,36,53], it was shown that these filters are much better described when beyond-mean-field correlations are taken into account. The same result is found here for δV_{pn}. The beyond-mean-field correlation energy is much smaller in a doubly magic nucleus than in its neighbors. Its rapid variation gives a contribution to δV_{pn} that pushes it to very large values in doubly magic nuclei, up to twice as large as the average trend.

At the same time, the pattern of the δV_{pn} values changes for doubly magic nuclei. For nuclei located either below or above the shell closures for both nucleon species, the experimental δV_{pn} tends to be *larger* than the average trend. In contrast, for nuclei where one nucleon species is below and the other above the respective shell closure, the experimental δV_{pn} value tends to be *smaller* than the average trend. This behavior is very well illustrated in Figs. 7, 8, and 9 for the shell closures at $Z = 50$ and $N = 82$.

In the literature, qualitative explanations have been proposed for this effect based on the nature of the orbitals filled by neutrons and protons. If the energies of both orbitals are larger or smaller [particle-particle (p-p) and hole-hole (h-h) cases] than that of the Fermi level, they are supposed to have a large overlap. On the contrary, if one of the energies is larger and the other smaller [particle-hole (p-h) and hole-particle (h-p) cases], this overlap is supposed to be small. The behavior of δV_{pn} is then attributed to the differences between the overlaps [21]. EDF calculations offer a different and more straightforward explanation. This effect results from the combination of a smooth macroscopic background and the contributions from deformation and beyond-mean-field correlation energies. As can be seen in Fig. 4, their combined absolute value increases in all directions around a doubly magic nucleus. Moreover, looking, for instance, at Figs. 5 and 6, one sees that this increase is nonlinear. The pattern that is observed for δV_{pn} around doubly magic nuclei is then a trivial consequence of the asymmetry of the relative signs of the four energies entering its definition. For example, for $N = 118$, the $Z = 74$ nucleus is located in such a way that the nonlinear increase of these contributions is pointing toward $N - 2$, $Z - 2$. For the same value of N but $Z = 78$ the isoenergy lines are nearly parallel to the N axis, and the contributions for a given Z value nearly cancel out.

Looking once more at Fig. 4, the picture on how δV_{pn} is built up emerges clearly. Let us divide the map into rectangles delimited by the proton and neutron magic numbers. In any of these rectangles, deformation and correlation energies grow nonlinearly from small values along all borders to large ones in the middle. The resulting map of deformation and correlation energies is highly symmetric and centered around the middle of the region. The definition of δV_{pn}, Eq. (1), however, is asymmetric. It is designed to probe the increase of the energy when going from the lower left to the upper right in the nuclear chart under the assumption that it is superimposed on a background of like-particle interactions independent of the number of the other particle. The combined deformation and dynamical correlation energy rarely follows this anticipated pattern. As a consequence, one always obtains positive contributions to δV_{pn} around the so-called p-p and h-h corners of the rectangle and negative values in the p-h and h-p corners. Close to the center of such a major-shell region, this trend is inverted when the deformation and correlation energies reach their maximum. This explanation of the pattern of δV_{pn} around shell closures does not invoke any knowledge about the spatial structure of the single-particle orbits and their overlaps and also indicates that the observed pattern of δV_{pn} does not necessarily signal stronger or weaker proton-neutron interactions in the four corners of a region of the nuclear chart between major shells.

The observation that the appearance of enhanced δV_{pn} values in the rare-earth region when going from ^{132}Sn to ^{208}Pb and beyond is correlated to the line of $N_{\text{valence}} \approx Z_{\text{valence}}$ has led the authors of Ref. [25] to the speculation that this phenomenon might be due to a "mini-Wigner energy" of origin similar to the Wigner energy that leads to enhanced δV_{pn} values along the $N = Z$ nuclei. Our analysis makes this scenario very unlikely and offers a simpler explanation. First, we underline that our model does not give any trace of the Wigner energy and its contribution to δV_{pn} at the $N = Z$ line, as is the case for all present-day self-consistent mean-field models [24,28,44], meaning that the relevant physics is not contained in it. In contrast, our model does reproduce very well the enhanced δV_{pn} values along the $N_{\text{valence}} \approx Z_{\text{valence}}$ line in the rare-earth region. As explained above, their enhancement is a consequence of the onset of deformation and beyond-mean-field correlations when going away from a doubly magic nucleus, which gives a positive contribution to δV_{pn} in some directions and negative in other directions due to the asymmetric definition of δV_{pn}.

C. Detailed analysis of δV_{pn} for selected nuclei

1. General comments

The discussion above demonstrates that the rapid variation of the deformation energy and the beyond-mean-field correlation energy from symmetry restoration and shape mixing often gives large contributions to $\delta V_{pn}(N, Z)$. For nuclei away from the $N = Z$ line, this variation is at the origin of almost all structures seen in the data. This also indicates that the assumption of a common single-particle basis made in Sec. II to obtain a simple expression for δV_{pn} in terms of proton-neutron matrix elements is rarely justified. When the structure of the four nuclei entering Eq. (1) is different, the question arises whether there are other terms in the energy functional than the proton-neutron interaction energy that contribute to δV_{pn}.

We have selected three representative nuclei for which we will decompose $\delta V_{pn}(N, Z)$ into contributions from the proton-proton, neutron-neutron, and proton-neutron terms in the EDF.

2. ^{208}Pb

The first nucleus ^{208}Pb has been chosen for two reasons. First, we have seen in Fig. 6 that the contribution of the beyond-mean-field correlation energy to the δV_{pn} value of this doubly magic nucleus is particularly large. Second, the spherical ^{208}Pb presents a very favorable situation to numerically test the frozen HF approximation, where the same set of single-particle wave functions is used to compute the energy of all four nuclei involved in the computation of δV_{pn}. As discussed in Sec. II A, this approximation has to be made to establish the direct relation between δV_{pn} and the two-body proton-neutron interaction. In fact, ^{208}Pb is one of the very few spherical nuclei for which such calculations can be performed. It requires that four neighboring nuclei have a closed-shell configuration, which is possible only for N and Z values for which the orbitals below the Fermi level are $p_{1/2^-}$ or $s_{1/2^+}$ levels for both protons and neutrons. These conditions are met for ^{208}Pb, with a ν $s_{1/2^+}$ level below $N = 126$ and a π $p_{1/2^-}$ level below $Z = 82$.

The results are presented in Table I. The four nuclei entering δV_{pn} have been calculated with the single-particle basis of ^{208}Pb (frozen HF approximation), without readjustment of the basis for each nucleus and without pairing correlations. Self-consistency for ^{206}Pb, ^{206}Hg, and ^{204}Hg has been considered for the results given in the HF column, and self-consistency and pairing correlations treated with the BCS + Lipkin Nogami

TABLE I. Decomposition of δV_{pn} into contributions coming from the different terms of the energy density functional for ^{208}Pb, namely, kinetic energy of neutrons and protons, the neutron-neutron, proton-proton, and proton-neutron parts of the Skyrme EDF, the neutron-neutron and proton-proton parts of the pairing functional, and the proton-proton Coulomb EDF. We also give the sum of all terms and the experimental value. All energies are in MeV.

	^{208}Pb			
Term	Frozen HF	HF	HF + BCS + LN	$J = 0$ GCM
Kinetic n	0.000	−0.056	−0.010	−0.105
Kinetic p	0.000	0.012	−0.044	−0.132
Skyrme n-n	0.025	0.076	−0.005	0.160
Skyrme p-p	0.017	−0.008	0.025	0.275
Skyrme p-n	0.162	0.211	0.218	0.382
Pairing n-n	...	...	0.027	−0.057
Pairing p-p	...	...	−0.005	−0.081
Coulomb	0.000	0.010	0.020	0.012
Total	0.204	0.245	0.225	0.457
$\delta V_{pn}^{\text{expt}}$	...	...		0.427

prescription have been taken into account for the values of the HF + BCS + LN column. Finally, the $J = 0$ projected GCM calculation is given in the last column.

We decompose the energy density functional into the kinetic energies of neutrons and protons (including the center-of-mass correction), the neutron-neutron, proton-proton, and proton-neutron parts of the Skyrme EDF that models the particle-hole part of the effective strong interaction, the neutron-neutron and proton-proton parts of the pairing functional, and the proton-proton Coulomb energy. The Skyrme and pairing functionals contain density-dependent terms. We interpret them as a density dependence of the respective neutron-neutron, proton-proton, and proton-neutron terms. This choice of decomposition is not unique, however. For further details about the functional, we refer to Refs. [32,54].

In the frozen HF calculation, the sole contribution to δV_{pn} comes from the Skyrme EDF. The neutron-proton terms give the largest contribution, although the neutron-neutron and proton-proton terms contribute about 20% through their density dependence. As soon as self-consistent wave functions are used, the one-body contribution from the kinetic energy becomes large. This is not surprising, as the kinetic energy provides a large contribution to the symmetry energy coefficient a_{sym} of the EDF [54,55], which, in turn, dominates the global trend of δV_{pn}, Eq. (12). All other terms in the functional are modified and can bring sizable contributions to δV_{pn}. Pairing correlations change all contributions even further. The final value of δV_{pn} from a self-consistent calculation results from a partial cancellation of several terms. The proton-neutron terms in the Skyrme functional are of the right order of magnitude and approach the final value of δV_{pn} within a given model, but even for ^{208}Pb, which is probably one of the most favorable cases for the frozen approximation, one can hardly conclude that δV_{pn} is a valuable measure of proton-neutron interactions.

More importantly, the spherical mean-field values are far from the experimental data and the correlations brought by symmetry restoration and configuration mixing are large and

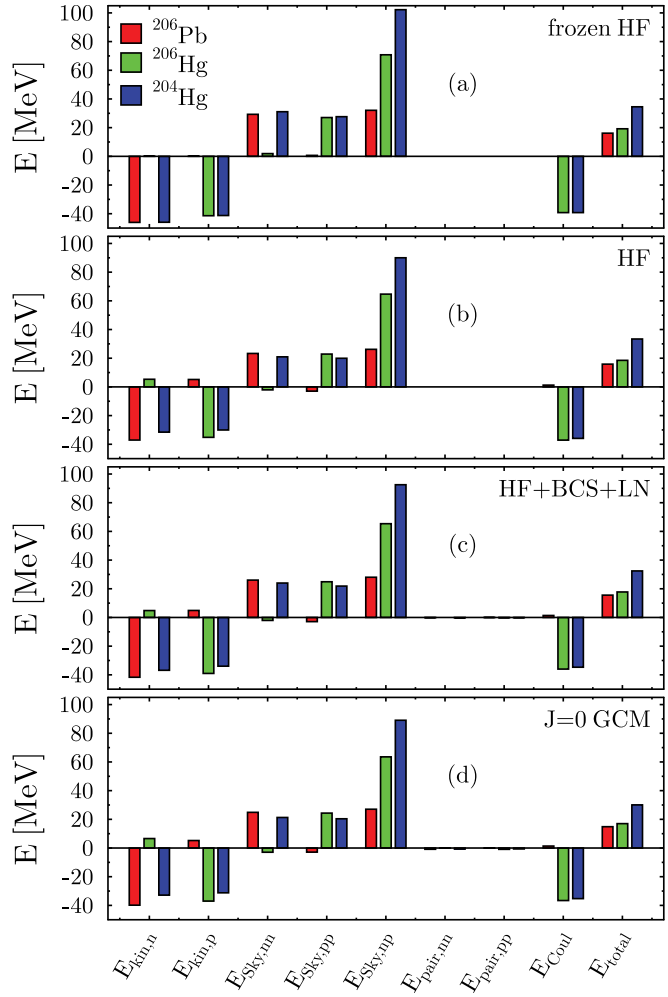

FIG. 12. (Color online) Difference between the values of the terms of the energy functional listed in Table I for ^{206}Pb, ^{206}Hg, and ^{204}Hg and their value for ^{208}Pb. The same four sets of calculations as in Table I are considered. All energies are in MeV.

crucial to obtain the correct value, as they increase δV_{pn} by 0.232 MeV to almost twice the mean-field value. The decomposition of the $J = 0$ projected GCM results is listed in Table I. All terms become large in absolute value but partially cancel each other. Their sum gives a value for δV_{pn} close to the data. This is not entirely surprising as correlation energy is always gained from the compensation between a loss in kinetic energy and a gain in interaction energy. Table I indicates that there are large contributions to δV_{pn} from proton-proton, neutron-neutron, and neutron-proton terms and that none of them is dominant.

Figure 12 illustrates how the δV_{pn} is built up from cancellations between the contributions of the four nuclei entering its definition. It shows the differences between the EDF terms defined in Table I for ^{206}Pb, ^{206}Hg, and ^{204}Hg and their value in ^{208}Pb. The contribution of a given term to δV_{pn} (^{208}Pb) is the sum of the values for ^{206}Pb (red) and ^{206}Hg (green) minus the value for ^{204}Hg (blue), divided by 4. While in the frozen HF approximation [Fig. 12(a)] most terms cancel out, exact self-consistency [Fig. 12(b)], pairing

TABLE II. Decomposition of δV_{pn} values for ^{168} Er and ^{152} Nd into contributions coming from the different terms in the energy density functional in deformed self-consistent mean-field calculations, namely, kinetic energy, the neutron-neutron, proton-proton and proton-neutron parts of the Skyrme EDF, pairing energy, and the proton-proton Coulomb EDF (see Table II). We also give the total contribution from beyond-mean-field correlations, the sum of all these terms, and the experimental value. All energies are in MeV.

Term	^{168}Er	^{152}Nd
Kinetic	−0.252	−0.334
Skyrme n-n	0.164	0.304
Skyrme p-p	0.065	−0.016
Skyrme n-p	0.372	0.676
Coulomb	0.005	−0.161
Pairing	−0.020	0.081
Total mean field	0.334	0.550
Correlation energy	−0.006	−0.051
$\delta V_{pn}^{\text{theo}}$	0.328	0.490
$\delta V_{pn}^{\text{expt}}$	0.362	0.509

[Fig. 12(c)], and collective quadrupole correlations [Fig. 12(d)] lead to a much more complex situation. One can conclude from this analysis that each contribution to δV_{pn} itself is the result of a partial compensation between changes in all four nuclei entering its definition.

3. *Deformed rare-earth nuclei*

Let us now consider two nuclei in a deformed region of the nuclear chart. The four nuclei entering the calculation of δV_{pn} for ^{168}Er have similar deformations. In contrast, they differ significantly for ^{152}Nd, as can be seen in Fig. 8. In both cases, the spherical mean-field results are of no interest and will not be discussed here. The contribution of correlations brought by configuration mixing and symmetry restoration is also small, and the analysis of δV_{pn} can be performed for the deformed calculations only. The value of δV_{pn} results from contributions coming from all terms in the functional. The kinetic energy brings a large negative contribution, even for ^{168}Er for which the four nuclei have very similar deformations. This demonstrates that the frozen approximation is not valid and that the use of a unique single-particle basis is not justified. The largest positive contribution to δV_{pn} comes from the Skyrme EDF. Other terms are small for ^{168}Er, but there is a large negative contribution of the Coulomb term in ^{152}Nd. Note also that, although the contribution of correlations is small for this nucleus, it has the right sign to bring the theoretical δV_{pn} in good agreement with the data.

Altogether, these examples indicate that, in a realistic model, δV_{pn} is not determined by the interaction between the last two valence nucleons but has contributions from the modifications of all single-particle wave functions on the one hand and from all terms in the energy functional on the other.

V. DISCUSSION AND CONCLUSIONS

In this paper, we have analyzed in detail the relevance of a difference between the binding energy of four nuclei, called δV_{pn}, as a measure of the proton-neutron interaction between valence particles and as an indicator for structural changes in nuclei.

We have first investigated whether one can derive a relation between δV_{pn} and a proton-neutron matrix element in simple models, where analytic formulas can be derived. Even in the oversimplified case where the four nuclei entering δV_{pn} can be described by HF wave functions generated by the same mean field and a two-body interaction, one obtains only a relation between δV_{pn} and a combination of two matrix elements. Any higher-order term in the interaction, such as a density dependence or a three-body interaction, complicates the relation, as do self-consistency and any correlation such as pairing, deformation, or any configuration mixing. This formal analysis already indicates that it can hardly relate δV_{pn} to any specific proton-neutron interaction in a realistic model. This formal analysis is confirmed by the decomposition of calculated δV_{pn} values for the doubly magic spherical ^{208}Pb nucleus and the deformed ^{152}Nd and ^{168}Er, for which we find, indeed, that all terms in the energy functional contribute, not just the proton-neutron interaction, and that self-consistency and correlations beyond the mean field play a substantial role.

We have then shown that our beyond-mean-field method has all the necessary ingredients to reproduce the global trends of δV_{pn}. As has been pointed out earlier [24], the global trend of δV_{pn} is determined by the symmetry and surface symmetry energy coefficients that can be deduced from an energy functional. With a detailed analysis of a few representative regions in the nuclear chart, we have illustrated how the fine structure of δV_{pn} builds up from the successive introduction of deformation and correlations due to symmetry restorations and configuration mixing. Both are crucial ingredients for the reproduction of data. As found earlier for two-nucleon separation energies [14,35,36], within our model it is essential to take into account beyond-mean-field correlations for the description of data in the vicinity of magic numbers. We have checked that the large-scale calculation of even-even nuclei using a mapped five-dimensional microscopic Bohr-Hamiltonian based on the Gogny force [56] gives qualitatively the same results as ours.

Our model provides a satisfactory description of the data, except at the $N = Z$ line, where the Wigner effect is absent from our results. Within the framework of our model, however, δV_{pn} provides neither a reliable *measure* of the proton-neutron interaction terms in the energy functional used nor a reliable *indicator* for structural changes. Certainly, in some instances structural changes such as the onset of deformation lead to anomalies in the δV_{pn} values, but in many other instances they do not, and there is no one-to-one correspondence between a structural change and the resulting modification of δV_{pn}. In turn, a local increase or decrease of δV_{pn} can have many different origins. One of the main limiting factors for the use of δV_{pn} as an indicator for structural change is its asymmetric definition, which results in the fact that additional binding from a change in nuclear structure contributes differently to δV_{pn} in sign and size depending on the direction in the nuclear chart in which the structure changes. In particular, the characteristic pattern of δV_{pn} having a significantly larger size for nuclei where only particles or only holes are added

to a doubly magic nucleus as compared to systems with particles added for one nucleon species and holes for the other (a pattern recently interpreted as a "mini-Wigner energy" [25]) is a trivial consequence of the asymmetric definition of δV_{pn} and *not* an indicator for a qualitative difference in either the proton-neutron interaction or a difference of their structure.

The usefulness of δV_{pn} is compromised by being a mass filter of very high order that is thereby prone to unpredictable cancellations when the nuclei entering δV_{pn} have different structure. Lower-order mass filters such as two-nucleon separation energies or Q values are usually more reliable indicators of structural changes than δV_{pn}, although these may fail as well. This also means that δV_{pn} does not provide a conclusive benchmark for nuclear EDF methods that would be superior or complementary to other mass filters such as two-nucleon separation energies and Q values.

ACKNOWLEDGMENTS

This work was supported by the "Interuniversity Attraction Pole" (IUAP) of the Belgian Scientific Policy Office under project P6/23. The computations were performed at the National Energy Research Scientific Computing Center, supported by the US Department of Energy under Contract No. DE-AC03-76SF00098 and using HPC resources from GENCI-IDRIS (Grant No. 2010-050707). The authors also thank R. V. F. Janssens and V. Hellemans for their critical reading of the manuscript.

[1] D. Lunney, J. M. Pearson, and C. Thibault, Rev. Mod. Phys. **75**, 1021 (2003).
[2] H.-J. Kluge, K. Blaum, and C. Scheidenberger, Nucl. Inst. Methods Phys. Res. A **532**, 48 (2004).
[3] K. Blaum, Phys. Rep. **425**, 1 (2006).
[4] H.-J. Kluge, Hyperfine Interact. **196**, 295 (2010).
[5] J. Duflo and A. P. Zuker, Phys. Rev. C **52**, R23 (1995); A. P. Zuker, Rev. Mex. Fis. S **54**, 129 (2008).
[6] P. Möller, J. R. Nix, W. D. Myers, and W. J. Swiatecki, At. Data Nucl. Data Tables **59**, 185 (1985); P. Möller, J. R. Nix, and K.-L. Kratz, *ibid.* **66**, 131 (1997).
[7] M. Samyn, S. Goriely, P.-H. Heenen, J. M. Pearson, and F. Tondeur, Nucl. Phys. A **700**, 142 (2002); S. Goriely, N. Chamel, and J. M. Pearson, Phys. Rev. Lett. **102**, 152503 (2009).
[8] S. Goriely, S. Hilaire, M. Girod, and S. Péru, Phys. Rev. Lett. **102**, 242501 (2009).
[9] O. Bohigas, X. Campi, H. Krivine, and J. Treiner, Phys. Lett. B **64**, 381 (1976).
[10] P.-G. Reinhard, M. Bender, W. Nazarewicz, and T. Vertse, Phys. Rev. C **73**, 014309 (2006).
[11] A. S. Jensen, P. G. Hansen, and B. Jonson, Nucl. Phys. A **431**, 393 (1984).
[12] J. G. Hirsch, A. Frank, and V. Velázquez, Phys. Rev. C **69**, 037304 (2004).
[13] J. Barea, A. Frank, J. G. Hirsch, and P. Van Isacker, Phys. Rev. Lett. **94**, 102501 (2005).
[14] M. Bender, G. F. Bertsch, and P.-H. Heenen Phys. Rev. C **78**, 054312 (2008).
[15] T. Otsuka, T. Suzuki, R. Fujimoto, H. Grawe, and Y. Akaishi, Phys. Rev. Lett. **95**, 232502 (2005).
[16] D. Von-Eiff, H. Freyer, W. Stocker, and M. K. Weigel Phys. Lett. B **344**, 11 (2005).
[17] G. A. Lalazissis, D. Vretenar, W. Pöschl, and P. Ring, Phys. Lett. B **418**, 7 (1998); Nucl. Phys. A **632**, 363 (1998).
[18] J.-Y. Zhang, R. F. Casten, and D. S. Brenner, Phys. Lett. B **227**, 1 (1989).
[19] D. S. Brenner, C. Wesselborg, R. F. Casten, D. D. Warner, and J.-Y. Zhang, Phys. Lett. B **243**, 1 (1990).
[20] R. B. Cakirli, D. S. Brenner, R. F. Casten, and E. A. Millman, Phys. Rev. Lett. **94**, 092501 (2005); **95**, 119903(E) (2005).
[21] R. B. Cakirli and R. F. Casten, Phys. Rev. Lett. **96**, 132501 (2006).
[22] D. S. Brenner, R. B. Cakirli, and R. F. Casten, Phys. Rev. C **73**, 034315 (2006).
[23] Y. Oktem, R. B. Cakirli, R. F. Casten, R. J. Casperson, and D. S. Brenner, Phys. Rev. C **74**, 027304 (2006).
[24] M. Stoitsov, R. B. Cakirli, R. F. Casten, W. Nazarewicz, and W. Satuła, Phys. Rev. Lett. **98**, 132502 (2007).
[25] R. B. Cakirli, K. Blaum, and R. F. Casten, Phys. Rev. C **82**, 061304(R) (2010).
[26] J. Jänecke, Phys. Rev. C **6**, 467 (1972); J. Jänecke and H. Behrens, Z. Phys. **256**, 236 (1972); Phys. Rev. C **9**, 1276 (1974); J. Jänecke and B. P. Eynon, Nucl. Phys. A **243**, 326 (1975); J. Jänecke and E. Comay, *ibid.* **436**, 108 (1985).
[27] P. Van Isacker, D. D. Warner, and D. S. Brenner, Phys. Rev. Lett. **74**, 4607 (1995).
[28] W. Satuła, D. J. Dean, J. Gary, S. Mizutori, and W. Nazarewicz, Phys. Lett. B **407**, 103 (1997).
[29] W. Greiner and J. A. Maruhn, *Nuclear Models* (Springer, Berlin, 1996).
[30] K. Heyde, C. De Coster, and J. Schietse, Phys. Rev. C **49**, 2499 (1994).
[31] E. Epelbaum, H.-W. Hammer, and U.-G. Meißner, Rev. Mod. Phys. **81**, 1773 (2009).
[32] M. Bender, P.-H. Heenen, and P.-G. Reinhard, Rev. Mod. Phys. **75**, 121 (2003).
[33] S. Typel and H. H. Wolter, Nucl. Phys. A **656**, 331 (1999).
[34] T. Niksic, D. Vretenar, P. Finelli, and P. Ring, Phys. Rev. C **66**, 024306 (2002).
[35] M. Bender, G. F. Bertsch, and P.-H. Heenen, Phys. Rev. Lett. **94**, 102503 (2005).
[36] M. Bender, G. F. Bertsch, and P.-H. Heenen, Phys. Rev. C **73**, 034322 (2006).
[37] See supplemental material at [http://link.aps.org/supplemental/10.1103/PhysRevC.73.034322] for tables with the intrinsic deformations and energies for 605 even-even nuclei.
[38] E. Chabanat, P. Bonche, P. Haensel, J. Meyer, and R. Schaeffer, Nucl. Phys. A **635**, 231 (1998); **643**, 441(E) (1998).
[39] V. M. Strutinsky, Nucl. Phys. A **95**, 420 (1967); **122**, 1 (1968).
[40] M. Brack and P. Quentin, Phys. Lett. B **56**, 421 (1975); Nucl. Phys. A **361**, 35 (1981).
[41] K. Heyde, *Basic Ideas and Concepts in Nuclear Physics* (Institute of Physics Publishing, Bristol, 2004).
[42] N. Zeldes, Phys. Lett. B **429**, 20 (1998).
[43] M. W. Kirson, Phys. Lett. B **661**, 246 (2008).

[44] E. Perlińska, S. G. Rohoziński, J. Dobaczewski, and W. Nazarewicz, Phys. Rev. C **69**, 014316 (2004).
[45] A. Poves and G. Martinez-Pinedo, Phys. Lett. B **430**, 203 (1998).
[46] D. D. Warner, M. A. Bentley, and P. Van Isacker, Nat. Phys. **2**, 311 (2006).
[47] E. Caurier, G. Martinez-Pinedo, F. Nowacki, A. Poves, and A. P. Zuker, Rev. Mod. Phys. **77**, 427 (2005).
[48] M. Breitenfeldt *et al.*, Phys. Rev. C **81**, 034313 (2010).
[49] S. Raman, C. W. Nestor Jr., and P. Tikkanen, At. Data Nucl. Data Tables **78**, 1 (2001).
[50] National Nuclear Data Center, information extracted from the NuDat 2 database [http://www.nndc.bnl.gov/nudat2/].
[51] K.-H. Schmidt, W. Faust, G. Münzenberg, H.-G. Clerc, W. Lang, K. Pielenz, D. Vermeulen, H. Wohlfarth, H. Ewald, and K. Güttner, Nucl. Phys. A **318**, 253 (1979).
[52] N. Zeldes, T. S. Dumitrescu, and H. S. Köhler, Nucl. Phys. A **399**, 11 (1983).
[53] P. Fleischer, P. Klüpfel, T. Cornelius, T. J. Bürvenich, S. Schramm, J. A. Maruhn, and P.-G. Reinhard, Eur. Phys. J. A **22**, 363 (2004).
[54] M. Bender, J. Dobaczewski, J. Engel, and W. Nazarewicz, Phys. Rev. C **65**, 054322 (2002).
[55] W. Satuła, R. A. Wyss, and M. Rafalski, Phys. Rev. C **74**, 011301(R) (2006).
[56] J.-P. Delaroche, M. Girod, J. Libert, H. Goutte, S. Hilaire, S. Péru, N. Pillet, and G. F. Bertsch, Phys. Rev. C **81**, 014303 (2010).